

Restitution in mapping models with an arbitrary amount of memory

Soma S. Kalb^{a)}

Department of Biomedical Engineering and Center for Nonlinear and Complex Systems, Duke University, Durham, North Carolina 27708

Elena G. Tolkacheva

Department of Physics and Center for Nonlinear and Complex Systems, Duke University, Durham, North Carolina 27708

David G. Schaeffer

Department of Mathematics and Center for Nonlinear and Complex Systems, Duke University, Durham, North Carolina 27708

Daniel J. Gauthier

Department of Physics, Department of Biomedical Engineering, and Center for Nonlinear and Complex Systems, Duke University, Durham, North Carolina 27708

Wanda Krassowska

Department of Biomedical Engineering and Center for Nonlinear and Complex Systems, Duke University, Durham, North Carolina 27708

(Received 10 September 2004; accepted 28 January 2005; published online 7 April 2005)

Restitution, the characteristic shortening of action potential duration (APD) with increased heart rate, has been studied extensively because of its purported link to the onset of fibrillation. Restitution is often represented in the form of mapping models where APD is a function of previous diastolic intervals (DIs) and/or APDs, $A_{n+1} = F(D_n, A_n, D_{n-1}, A_{n-1}, \dots)$, where A_{n+1} is the APD following a DI given by D_n . The number of variables previous to D_n determines the degree of memory in the mapping model. Recent experiments have shown that mapping models should contain at least three variables (D_n, A_n, D_{n-1}) to reproduce a restitution portrait (RP) that is qualitatively similar to that seen experimentally, where the RP shows three different types of restitution curves (RCs) [dynamic, S1–S2, and constant-basic cycle length (BCL)] simultaneously. However, an interpretation of the different RCs has only been presented in detail for mapping models of one and two variables. Here we present an analysis of the different RCs in the RP for mapping models with an arbitrary amount of memory. We determine the number of variables necessary to represent the different RCs in the RP. We also present a graphical visualization of these RCs. Our analysis reveals that the dynamic and S1–S2 RCs reside on two-dimensional surfaces, and therefore provide limited information for mapping models with more than two variables. However, constant-BCL restitution is a feature of the RP that depends on higher dimensions and can possibly be used to determine a lower bound on the dimensionality of cardiac dynamics. © 2005 American Institute of Physics. [DOI: 10.1063/1.1876912]

Mathematical models that describe cardiac dynamics are important tools in understanding lethal cardiac arrhythmias, such as ventricular fibrillation. One approach to modeling is to attempt to reproduce the physiological ionic fluxes and changes in concentration across the cell membrane. However, analysis of such multidimensional models is very difficult. In contrast, mapping models, which relate the duration of the action potential (APD) to a number of previous diastolic intervals (DIs) and/or APDs, lend themselves to analysis. In fact, much of the practical theory regarding the onset of instability of heart rhythms is based on analysis of the most simple mapping where APD is a function of only the previous DI. This relationship between APD and preceding DI is measured experimentally using various pacing protocols, yielding

so-called restitution curves (RCs). Recent experiments have demonstrated that the most simple mapping model is inadequate to describe the different RCs, and that memory (dependence on more previous APDs/DIs) must be included in mapping models. However, it is not well understood how to interpret different experimental RCs for mapping models with higher degrees of memory. In this paper, we examine mapping models with an arbitrary amount of memory to interpret the different RCs measured experimentally and to derive expressions for their slopes. We use a graphical visualization to aid in this presentation. Our analysis demonstrates the limitations and advantages of existing protocols and RCs, which may be useful in the design of new protocols that take into account the multidimensional nature of memory in cardiac tissue.

^{a)}Electronic address: ss49@duke.edu

I. INTRODUCTION

Sudden cardiac death, usually due to ventricular fibrillation, claims the lives of as many as 400 000 people each year in the United States alone. In order to understand the cause of ventricular fibrillation, as well as other cardiac arrhythmias, the dynamical properties of the heart have been studied using mathematical models of various forms. For example, ionic models¹⁻³ attempt to reproduce cardiac dynamics by characterizing the concentration differences and ionic fluxes across the cardiac cell membrane as determined by experimental data. These multidimensional models are fairly complex, often with more than 20 state variables, which makes analysis of such models difficult.

Another approach is to examine cardiac dynamical behavior, rather than individual ionic processes. One such behavior that has been studied extensively is restitution, the characteristic shortening of action potential duration (APD) with increased heart rate. In pioneering work by Nolasco and Dahlen⁴ and Guevara *et al.*,⁵ restitution was described as a one-dimensional mapping model

$$A_{n+1} = F(D_n), \quad (1)$$

where A_{n+1} is the APD following a diastolic interval (DI) D_n .

While analysis of this simple model yields much insight into possible mechanisms for abnormal cardiac rhythms, restitution has proved to be more complex than originally proposed. For example, it has been shown that the functional relationship given in (1), known as the restitution curve (RC), depends on the pacing protocol used to obtain it,^{6,7} a phenomenon known as rate-dependent restitution. Experimentally, two pacing protocols are commonly used to investigate cardiac restitution, the dynamic and the S1-S2. Recently, a new protocol was introduced that measures the less-known constant-BCL (CB) RC (Ref. 8) (see Sec. II for more detail regarding the CB RC). It was shown that these RCs describe different aspects of cardiac dynamics: the steady-state response, responses to perturbations, and transient responses. Moreover, it was shown that simultaneous measurement of all RCs at each basic cycle length (BCL) allows more complete characterization of cardiac dynamics and possible prediction of the onset of instability.

The new protocol, called the *perturbed downswEEP protocol*, was implemented experimentally in a bullfrog heart preparation.⁹ The resulting responses were plotted in a *restitution portrait* (RP), which simultaneously displays several RC segments at each BCL, as well as transient responses, instead of only a single RC. Analysis of the experimental RP revealed that a mapping model of the form (1) cannot reproduce many features of the experimental RP. However, a mapping model of the form

$$A_{n+1} = F(D_n, A_n, D_{n-1}) \quad (2)$$

exhibits an RP that is qualitatively similar to that seen experimentally. The mapping model of the form (2) is considered to have short-term memory in that the response depends on the pacing history (a number of previous DIs and/or APDs). Mapping models of the form (2) have been formulated to phenomenologically represent memory,^{10,11} and have also been derived as an asymptotic approximation of a sim-

plified ionic model.¹² The short-term memory included in these models allows them to reproduce experimental observations, such as rate dependence, that are not produced by the memoryless mapping model (1).

Given the fact that a three-variable model of the form (2) reproduces important cardiac behaviors, it is important to understand the physical significance of the experimentally measured RCs for such a memory model. An interpretation of different RCs was presented previously⁸ for a two-variable model of the form

$$A_{n+1} = F(D_n, A_n), \quad (3)$$

shedding light on the origins of rate-dependent restitution. However, extension of that analysis for a three-variable model is not transparent. Moreover, although the mapping model (2) produced an RP that was qualitatively similar to experiments, quantitative agreement was not obtained. In addition, the three-variable model breaks down in trying to predict the onset of alternans. Therefore, higher-dimensional models with even more memory variables may be required in order to obtain quantitative agreement with the RP and to predict alternans. Thus, an understanding of the meaning of different RCs for models with greater amounts of memory (i.e., more than two variables) is necessary to design useful pacing protocols and to continue to use restitution as a tool for analyzing cardiac dynamics.

Here, we examine restitution for mapping models with an *arbitrary* amount of memory, i.e., any model that can be represented in the general form

$$A_{n+1} = F(D_n, A_n, D_{n-1}, A_{n-1}, D_{n-2}, \dots). \quad (4)$$

Therefore, this analysis applies to the one-, two-, and three-variable models already mentioned, as well as to any future models with more memory variables that may emerge. This analysis is performed in the context of the RP and therefore focuses on the 1:1 regime of possible responses. First, we describe the components of the RP as they apply to models of the form (4). Next, we interpret each of the various RCs in terms of these higher-dimensional models. Finally, we present a graphical visualization of the RCs for such models, and a specific example of this visualization for a model of the form (2). We find that, in addition to aiding in the comprehension of restitution for complex mapping models, our analysis demonstrates the limitations of the commonly used dynamic and S1-S2 protocols and uncovers the potential advantages of measuring CB restitution.

II. THE RESTITUTION PORTRAIT

The analysis in this paper is presented in the context of the RP, which simultaneously shows a dynamic RC, segments of S1-S2 RCs, and CB transient responses. To produce an RP, stimuli are applied according to the perturbed downswEEP protocol and APD is plotted as a function of previous DI for all responses. An example of an RP is shown in Fig. 1. The details of the perturbed downswEEP protocol and the RP have been described in detail previously.⁹ Briefly, in this protocol, BCL is decreased in a downswEEP. At each BCL in the downswEEP, once steady state is achieved, perturbations are applied at $BCL + \delta$ and at $BCL - \delta$ before de-

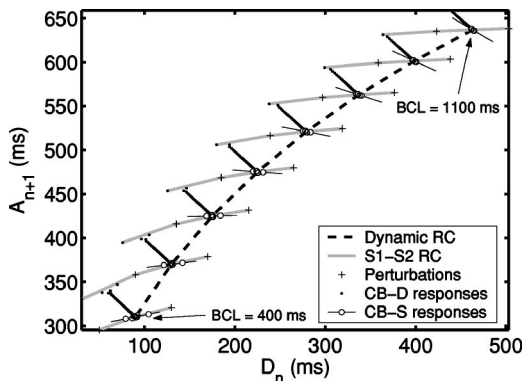


FIG. 1. An RP produced by iteration of the mapping (A4) given in the Appendix. BCL was decreased from 1100 to 400 ms in 100 ms increments. At each BCL, perturbations were applied at $BCL \pm 40$ ms. CB-S responses do not fall on a single line. The line drawn through the CB-S responses, which is a least-squares fit to the responses, emphasizes that the CB responses do not fall on the S1-S2 RC segment. This can be seen more clearly in a close-up for a single BCL in Fig. 2.

creasing the BCL for the next step in the downswEEP. In between the 2 perturbations, pacing resumes at the current BCL until the response returns to steady state.

Figure 2 shows the details of the RP for a single BCL in the downswEEP. As shown in this figure, in applying the protocol, two different RCs are produced, the dynamic and the S1-S2. The dynamic RC describes steady-state responses over all BCLs. In Fig. 2, the steady-state response, also known as the fixed point, corresponds to the intersection of the RCs. The S1-S2 RC segment shows responses to the perturbations. Note that the S1-S2 RC segment in the RP represents only a portion of a conventional S1-S2 RC around the fixed point (the point where the perturbation is equal to zero).

The CB transients are a feature of the RP that have only been described in detail for the two-variable model of the form (3). Here, we clarify their meaning for mapping models with more memory. The CB transient responses are all responses that occur while pacing at a constant BCL. In particular for the RP, CB-D responses are those that occur after a sustained change in BCL (Fig. 2, filled circles). The CB-S responses are the transient responses after each of the perturbations is applied (open circles). For a two-variable mapping

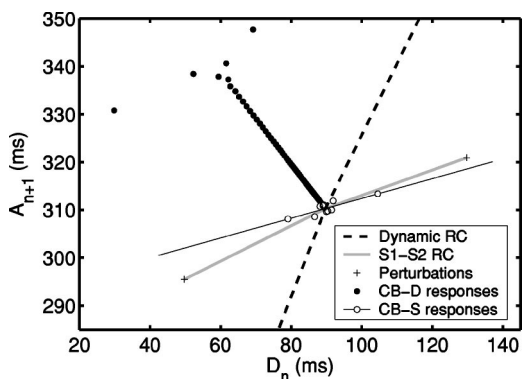


FIG. 2. Details of the RP shown in Fig. 1 for a single BCL (BCL = 400 ms).

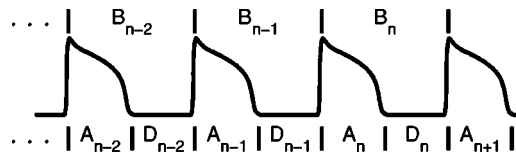


FIG. 3. For mapping models of the form (4), the duration of the $(n+1)^{st}$ action potential A_{n+1} is a function of previous DIs and APDs as shown in the figure. The BCLs are shown above the action potentials.

model of the form (3), all CB transient responses (CB-D and CB-S) fall on a single curve, which was defined as the CB RC.⁸ However, for models with higher degrees of memory, CB responses do not fall on a single curve, as shown in Figs. 1 and 2.¹³ Therefore, in this paper, the responses to constant pacing are referred to as “CB transients,” rather than a CB RC.

III. RESTITUTION CURVES FOR HIGHER-DIMENSIONAL MODELS

For the following analysis, we consider mapping models in which APD is described as a function of a number of previous sequential DIs and/or APDs in the form (4), where $A_n + D_n = B_n$, as depicted in Fig. 3. In this paper, the degree of memory is determined by the number of variables in the argument for F . The one-variable model $A_{n+1} = F(D_n)$ is considered a memoryless model, whereas the two-variable model $A_{n+1} = F(D_n, A_n)$ has one degree of memory. We refer to arguments involving either a DI or an APD as “D variables” and “A variables,” respectively.

A. The dynamic restitution curve

To examine the dynamic RC, we use the fact that the dynamic RC consists of the steady-state responses over all BCLs. At steady state, the following conditions apply:

$$D_n = D_{n-1} = D_{n-2} = \dots = D_*, \tag{5}$$

$$A_{n+1} = A_n = A_{n-1} = A_{n-2} = \dots = A_*, \tag{6}$$

where A_* and D_* represent the steady-state values of APD and DI. By substituting the variables D_* and A_* into (4), we can write

$$A_* = F(D_*, A_*, D_*, A_*, D_*, \dots) = \Psi(D_*, A_*). \tag{7}$$

Equation (7) is an implicit expression for the dynamic RC. The steady-state values of D_* and A_* for any BCL B are determined by solving (7) for D_* and A_* with the condition $D_* = B - A_*$. Therefore, for the dynamic RC, a higher-dimensional mapping can be reduced to a two-dimensional function Ψ .

In the RP, the dynamic RC is obtained by plotting A_* as a function of D_* . Therefore, the slope of the dynamic RC at any fixed point is given as

$$S_{\text{dyn}} \equiv \left. \frac{\partial A_*}{\partial D_*} \right|_{\text{fp}} = \left. \frac{\partial F}{\partial D_*} \right|_{\text{fp}}, \tag{8}$$

where fp denotes evaluation at the fixed point. The right-hand side of (8) results from the fact that $A_* = A_{n+1} = F$. By

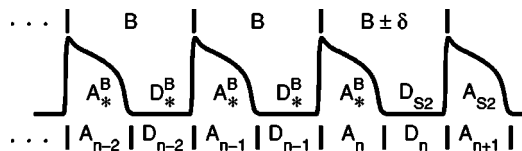


FIG. 4. Responses during the application of a perturbation to determine the S1–S2 RC. All variables previous to D_n are at the steady-state for the BCL B . The S2 response is given by (D_{S2}, A_{S2}) .

differentiating (4) with respect to D_* by the chain rule, we obtain

$$\begin{aligned} \frac{\partial F}{\partial D_*} &= \frac{\partial F}{\partial D_n} \frac{\partial D_n}{\partial D_*} + \frac{\partial F}{\partial A_n} \frac{\partial A_n}{\partial A_*} \frac{\partial A_*}{\partial D_*} + \frac{\partial F}{\partial D_{n-1}} \frac{\partial D_{n-1}}{\partial D_*} \\ &+ \frac{\partial F}{\partial A_{n-1}} \frac{\partial A_{n-1}}{\partial A_*} \frac{\partial A_*}{\partial D_*} + \dots, \end{aligned} \quad (9)$$

where the expression extends for all variables in the model. Note that the partial derivatives of the D variables and the A variables with respect to D_* and A_* , respectively, are equal to one by (5) and (6). Therefore, by rearranging terms and solving for $\partial A_*/\partial D_*$, we obtain the following expression for the slope of the dynamic RC:

$$S_{\text{dyn}} = \frac{(\partial F/\partial D_n + \partial F/\partial D_{n-1} + \partial F/\partial D_{n-2} + \dots)|_{\text{fp}}}{1 - (\partial F/\partial A_n + \partial F/\partial A_{n-1} + \partial F/\partial A_{n-2} + \dots)|_{\text{fp}}}, \quad (10)$$

where the numerator is the sum of all partial derivatives of F with respect to the D variables, and the expression enclosed in parentheses in the denominator is the sum of the partial derivatives of F with respect to the A variables in the model. For a one-variable model, there is only one RC, regardless of the protocol, and therefore, $S_{\text{dyn}} = dF/dD_n$, as expected. For two- and three-variable models, the expressions for S_{dyn} given previously^{8,14} are special cases of (10).

Thus, the dynamic RC can be expressed in terms of only two variables, A_* and D_* , which are determined from all of the variables in the mapping. In this sense, the explicit functional dependence of the dynamic RC on any one of the individual memory terms is lost. Additionally, the slope S_{dyn} for the mapping model (4) has a form given by (10) regardless of the amount of memory in the model and depends on the derivatives of F with respect to all of the A and D variables in the model. Hence, S_{dyn} depends on the degree of memory in the model.

B. The S1–S2 restitution curve

As a result of rate-dependent restitution, the S1–S2 RC depends on the S1–S1 BCL used to generate it. Figure 4 shows the stimuli and responses obtained during a part of the perturbed downswEEP protocol when a perturbation is applied for a particular BCL B . We note that in the perturbed downswEEP protocol (or a conventional S1–S2 protocol), the perturbation (S2 stimulus) is applied after the response has reached steady state at B , with the steady-state response given by (D_*^B, A_*^B) . The responses to the perturbations

(D_{S2}, A_{S2}) form the S1–S2-RC segments in the RP, where $D_{S2} = D_*^B \pm \delta$. The response A_{S2} , can be determined from the mapping (4), by noting the following:

$$A_{n+1} = A_{S2}, \quad (11)$$

$$D_n = D_{S2}, \quad (12)$$

$$A_n = A_{n-1} = A_{n-2} = \dots = A_*, \quad (13)$$

$$D_{n-1} = D_{n-2} = \dots = D_*, \quad (14)$$

$$A_* = B - D_*, \quad (15)$$

$$D_* \equiv D_*^B. \quad (16)$$

Equations (13)–(16) result from the fact that the S2 stimulus is applied after steady state has been reached, and therefore all variables previous to the first variable (D_n) are at steady state. Note that in (16), D_*^B is considered a constant equal to the steady-state DI for that BCL. To signify that it is a constant, it is written in a roman typeface, rather than in italics. Therefore, the S1–S2 RC is given by substituting equations (11)–(16) into (4),

$$\begin{aligned} A_{S2} &= F(D_{S2}, B - D_*, D_*, B - D_*, D_*, \dots)|_{D_* = D_*^B} \\ &= \Omega(D_{S2}, D_*)|_{D_* = D_*^B}. \end{aligned} \quad (17)$$

Thus, for a given BCL B , the S1–S2 RC is given by the function Ω , and depends only on the first D variable and the steady-state DI, regardless of the number of memory variables in the mapping model.

In the RP, the S1–S2 RC is obtained by plotting the pairs (D_{S2}, A_{S2}) , with D_{S2} as the independent variable. Therefore, the slope of the S1–S2 RC at the fixed point is given by

$$S_{12} = \left. \frac{\partial A_{S2}}{\partial D_{S2}} \right|_{\text{fp}} = \left. \frac{\partial F}{\partial D_{S2}} \right|_{\text{fp}}, \quad (18)$$

where the right-hand side of (18) results from the fact that $A_{S2} = A_{n+1} = F$. By differentiating (4) with respect to D_{S2} , we obtain

$$\begin{aligned} \frac{\partial F}{\partial D_{S2}} &= \frac{\partial F}{\partial D_n} \frac{\partial D_n}{\partial D_{S2}} + \frac{\partial F}{\partial A_n} \frac{\partial A_n}{\partial D_{S2}} + \frac{\partial F}{\partial D_{n-1}} \frac{\partial D_{n-1}}{\partial D_{S2}} \\ &+ \frac{\partial F}{\partial A_{n-1}} \frac{\partial A_{n-1}}{\partial D_{S2}} + \dots \end{aligned} \quad (19)$$

Note that $\partial D_n/\partial D_{S2} = 1$, while the partial derivatives of all previous A and D variables with respect to D_{S2} are equal to zero because they do not depend on D_{S2} . Therefore, the slope of the S1–S2 RC for a mapping model with an arbitrary number of memory variables is given by

$$S_{12} = \left. \frac{\partial F}{\partial D_n} \right|_{\text{fp}}. \quad (20)$$

The slope of the S1–S2 RC is determined by Eq. (20) regardless of the number of A and D variables in the mapping model (4), and thus does not depend on the amount of memory in the model. However, the values of the S1–S2 RC do depend on the amount of memory in the model, because

the steady-state values of APD and DI for a given BCL depend on all of the A and D variables in the model as described in Sec. III A.

In some ionic models, such as the Beeler–Reuter and Luo–Rudy phase 1 models, S_{12} has been shown to predict the onset of instability.^{15–18} Presumably, this is because there is little memory present in such models. For the memoryless mapping model given by (1), the criterion for stability of the 1:1 response predicts that alternans will occur when $|F'(D_n)| \geq 1$.⁵ Thus, according to (20), S_{12} can be used to assess stability for memoryless models. Incidentally, S_{dyn} and S_{12} will be equivalent for memoryless models because the RC obtained will be the same for any pacing protocol.

C. Transient CB responses

The RP includes transient responses in addition to the RCs mentioned above. These transients are obtained during constant pacing at a BCL B either for a decrease in BCL in the downsweep, or for recovery from a perturbation. The full mapping F can be reduced for these CB responses by noting that $A_m + D_m = B$ for $m = n, n-1, n-2, \dots$. Therefore, during pacing at a constant BCL B , the following holds:

$$\begin{aligned} A_{n+1} &= F(D_n, B - D_n, D_{n-1}, B - D_{n-1}, D_{n-2}, \dots) \\ &= \Phi(D_n, D_{n-1}, D_{n-2}, \dots), \end{aligned} \quad (21)$$

i.e., during constant pacing, A_{n+1} depends only on the D vari-

ables in the model. In the RP, A_{n+1} is plotted versus D_n . For models with one D variable, such as those considered by Tolkacheva *et al.*^{8,19} and Gilmour and collaborators,^{20,21} all CB responses will fall on the curve given by $A_{n+1} = \Phi(D_n)$. For models with more than one D variable of memory, such as that considered by Chialvo *et al.*¹⁰ and Fox *et al.*,²² the responses will not fall necessarily on a single curve in the RP due to the dependency of Φ on previous D variables.

Whereas the RCs described previously in Secs. III A and III B are given by exact expressions, the sequence of CB responses is only determined by iterating the model. However, insight into the expected dynamics can be gained by determining the eigenvalues and eigenvectors of the mapping Φ . Eigenvalues and eigenvectors can be determined by first linearizing around the fixed point (D_*, A_*) ,

$$\begin{aligned} A_{n+1} = A_* + & \left. \frac{\partial \Phi}{\partial D_n} \right|_{\text{fp}} (D_n - D_*) + \left. \frac{\partial \Phi}{\partial D_{n-1}} \right|_{\text{fp}} (D_{n-1} - D_*) \\ & + \left. \frac{\partial \Phi}{\partial D_n} \right|_{\text{fp}} (D_{n-2} - D_*) + \dots, \end{aligned} \quad (22)$$

where fp denotes evaluation at the fixed point. Rewriting (22) in terms of deviations from the fixed point $\delta_n = D_n - D_*$, we obtain

$$\begin{pmatrix} \delta_{n+1} \\ \delta_n \\ \delta_{n-1} \\ \vdots \end{pmatrix} = \begin{pmatrix} -\left. \frac{\partial \Phi}{\partial D_n} \right|_{\text{fp}} & -\left. \frac{\partial \Phi}{\partial D_{n-1}} \right|_{\text{fp}} & -\left. \frac{\partial \Phi}{\partial D_{n-2}} \right|_{\text{fp}} & \cdots \\ 1 & 0 & 0 & \cdots \\ 0 & 1 & 0 & \cdots \\ \vdots & \vdots & \vdots & \cdots \end{pmatrix} \begin{pmatrix} \delta_n \\ \delta_{n-1} \\ \delta_{n-2} \\ \vdots \end{pmatrix}. \quad (23)$$

In (23), the square matrix is $m \times m$, where m is the number of D variables in the mapping model. The first row of this matrix consists of the partial derivatives of Φ with respect to each of the D variables (with a negative sign). The remaining rows are zeros with the exception of the lower off-diagonal elements which have a value of 1. Eigenvalues and eigenvectors of this matrix can be determined by standard eigen-system analysis. Also, due to the form of this matrix, determination of its characteristic polynomial is straightforward. Therefore, criteria for stability can be determined by imposing conditions on the eigenvalues in the characteristic polynomial, as demonstrated previously for two- and three-variable models.^{8,14} In these previous studies, analytical formulations for the stability criteria were expressed in terms of the RC slopes. For models with more than three variables, further analysis, and possibly the development of a new pacing protocol, will be required to determine how to relate the analytical expression for stability to quantities that can be measured experimentally.

The behavior of the CB responses for a given BCL is governed by the eigenvalues and eigenvectors of the square matrix in Eq. (23) and is illustrated by example in Sec. IV C. This example will show that the dynamics of the mapping model (4) depends on m , the number of D variables (and eigenvalues) in the model. In particular, m determines the dimension of the space where the CB responses reside, which affects the appearance of the CB responses in the RP.

IV. VISUALIZATION

In this section, we present a graphical visualization to demonstrate the relationship between the mapping model F and the components of the RP. We apply certain restrictions to the mapping model, such as those presented in the preceding sections, to allow determination of the surfaces that contain each of the RP components. To generate the plots used in this visualization, we used a three-variable mapping model of the form (2), given as Eq. (A4) in the Appendix. However, unless otherwise noted, this visualization technique can be

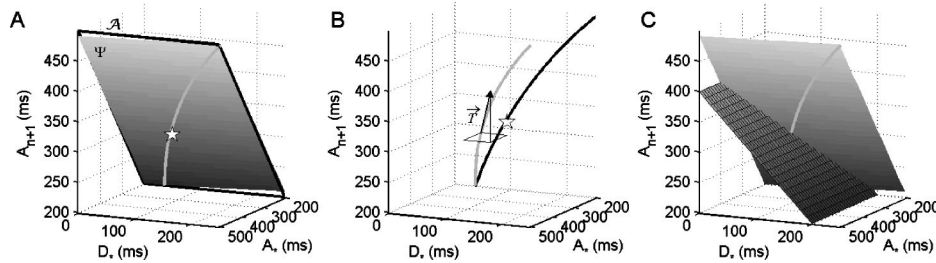


FIG. 5. Visualization of the dynamic RC. (A) The intersection of the surfaces Ψ and \mathcal{A} forms the 3D-DRC (light gray trace). Note that the surfaces Ψ and \mathcal{A} are at a shallow angle to one another. (B) The projection (black) of the 3D-DRC (gray) onto the $(A_{n+1}-D_*)$ plane gives the conventional dynamic RC. The vector \vec{T} is tangent to the 3D-DRC at the fixed point for the BCL $B=400$ ms. \vec{T} is scaled in magnitude for viewing purposes. (C) The surface Ψ intersected by the hatched plane defined by (25), where $B=400$ ms. The stars in (A) and (B) indicate the steady-state response for the BCL $B=400$ ms as determined by this intersection. The particular form of Ψ used for this visualization is given as (A5) in the Appendix.

generalized for mapping models with arbitrarily many degrees of memory.

A. The dynamic restitution curve

As presented in Sec. III A, for the dynamic RC, a mapping F with an arbitrary number of memory variables is reduced to an expression of only steady-state pairs (D_*, A_*) . These pairs reside on a two-dimensional surface defined by the function Ψ with A_* and D_* as independent variables, as shown in Fig. 5. In this plot, the vertical axis represents A_{n+1} . The dynamic RC is then determined by noting that at steady-state, the following condition holds:

$$A_{n+1} = A_*. \quad (24)$$

Therefore the dynamic RC is determined by the intersection of the surface Ψ with the plane \mathcal{A} defined by (24). This plane is outlined in black in Fig. 5(a), and its intersection with Ψ is shown as the solid gray curve. The solid gray curve is the dynamic RC in three-dimensional space, and will be abbreviated 3D-DRC. However, RCs are typically viewed in two dimensions, specifically in the $(A_{n+1}-D_n)$ plane. Therefore, the conventional dynamic RC is the projection of the 3D-DRC onto the $(A_{n+1}-D_n)$ plane, or in this case, the $(A_{n+1}-D_*)$ plane [Fig. 5(b)]. Note that there is only one dynamic RC over all BCLs.

The steady-state response for a given BCL B is determined by the pacing relation

$$A_n = B - D_n. \quad (25)$$

For the axes shown in Fig. 5, the pacing relation corresponds to a plane defined by $A_{n+1} = B - D_*$, and the steady-state response for that BCL is given by the intersection of the 3D-DRC with that plane. This intersection is shown in Fig. 5(c). The stars shown on the curve in Figs. 5(a) and 5(b) correspond to this intersection.

1. Graphical determination of S_{dyn}

To determine S_{dyn} , we must find a vector that is tangent to the dynamic RC at the fixed point. We will first determine a vector tangent to the 3D-DRC as illustrated in Fig. 5(b), and then project that vector onto the $(A_{n+1}-D_*)$ plane. When two surfaces intersect to form a curve, a vector that is tangent to this curve at any point is given by the cross product of the

normal vectors to the surfaces at that point. A normal vector of the surface Ψ at any fixed point is the gradient of the level surface given by $S_{\Psi}(A_*, D_*, A_{n+1}) = \Psi(A_*, D_*) - A_{n+1} = 0$,

$$\nabla S_{\Psi} = \left. \frac{\partial \Psi}{\partial A_*} \right|_{\text{fp}} \hat{i} + \left. \frac{\partial \Psi}{\partial D_*} \right|_{\text{fp}} \hat{j} - \hat{k}, \quad (26)$$

where \hat{i} , \hat{j} , and \hat{k} are the unit vectors in the positive A_* , D_* , and A_{n+1} directions, respectively. Similarly, the normal vector of the surface \mathcal{A} is given by

$$\nabla \mathcal{A} = \hat{i} - \hat{k}. \quad (27)$$

The cross product yielding the tangent vector \vec{T} at any fixed point is then given by

$$\begin{aligned} \vec{T} = \nabla S_{\Psi} \times \nabla \mathcal{A} = & - \left. \frac{\partial \Psi}{\partial D_*} \right|_{\text{fp}} \hat{i} + \left(\left. \frac{\partial \Psi}{\partial A_*} \right|_{\text{fp}} - 1 \right) \hat{j} \\ & - \left. \frac{\partial \Psi}{\partial D_*} \right|_{\text{fp}} \hat{k}. \end{aligned} \quad (28)$$

Therefore, the vector given in (28) is tangent to the 3D-DRC at the fixed point, as shown in Fig. 5. The projection of \vec{T} onto the $(A_{n+1}-D_*)$ plane is given by its \hat{j} and \hat{k} components and yields the tangent to the dynamic RC at the desired fixed point. Therefore, the slope is given by the ratio of the \hat{k} component to the \hat{j} component, or

$$S_{\text{dyn}} = \frac{\partial \Psi / \partial D_*|_{\text{fp}}}{1 - \partial \Psi / \partial A_*|_{\text{fp}}}. \quad (29)$$

Equation (29) is equivalent to the expression (10) for S_{dyn} derived earlier by the chain rule.

This graphical visualization demonstrates that the surface Ψ containing the 3D-DRC can be represented in two dimensions, as a function of D_* and A_* . However, D_* and A_* are determined from all the variables in the mapping model; therefore the shape of Ψ , and thus the slope S_{dyn} , depends on the memory in the mapping model.

B. The S1-S2 restitution curve

According to (17), the S1-S2 RC for a given BCL depends only on the first D variable and the steady-state response, regardless of the degree of memory. To visualize this, the function Ω can be plotted as a two-dimensional

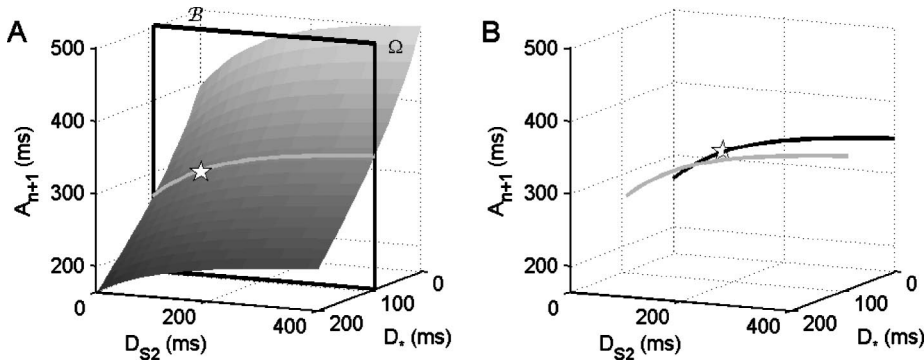


FIG. 6. Visualization of the S1-S2 RC. (A) The shaded surface is the surface Ω . The outlined plane is the plane B . The intersection of these two surfaces (light gray trace) forms the 3D-SRC. (B) The projection (black) of the 3D-SRC (gray) onto the $(A_{n+1}-D_{S2})$ plane yields the conventional S1-S2 RC. The stars indicate the value of the S1-S2 RC when $D_n=D_*^B$. The specific form of Ω is given as (A7) in the Appendix.

surface, where D_{S2} and D_* are independent variables [Fig. 6(a)]. This surface describes A_{n+1} as a function of D_{S2} for various steady-state D_* values. However, for a given BCL, D_* has a certain value as determined by the dynamic RC. Therefore, the S1-S2 RC is determined by intersecting the surface Ω with the plane B defined by

$$D_* \equiv D_*^B. \tag{30}$$

This intersection (shown as the heavy gray curve in Fig. 6) is the S1-S2 RC in three dimensions (3D-SRC). The 3D-SRC is projected onto the $(A_{n+1}-D_{S2})$ plane to yield the conventional S1-S2 RC [Fig. 6(b)]. Note that a different surface Ω exists for every B , yielding a different RC for each S1-S1 pacing interval. The star shown in Fig. 6 shows the steady-state response, when $D_{S2}=D_*^B$, and corresponds to the star in Fig. 5.

1. Graphical determination of S_{12}

The 3D-SRC is parallel to the $(A_{n+1}-D_n)$, or $(A_{n+1}-D_{S2})$ plane. Therefore it follows that the slope of the S1-S2 RC at the fixed point is given by the partial derivative of Ω in the D_{S2} direction, or

$$S_{12} = \left. \frac{\partial \Omega}{\partial D_{S2}} \right|_{fp}. \tag{31}$$

Equation (31) is equivalent to (20) by the chain rule. Note that in Fig. 6, the shape of the surface Ω in D_{S2} direction, and thus the expression for S_{12} , does not depend on the amount of memory in the mapping model (4). All memory is manifest in the D_* direction, and is involved in determining APD values for the S1-S2 RC, but not the slope S_{12} .

C. CB transient

As presented in Sec. III C, the function Φ describing transient CB responses is m dimensional, where m is the number of D variables in the mapping model. Therefore, Φ can only be presented graphically for $m \leq 2$. Here, we present a visualization for the specific model given in the Appendix (A4), which has two D variables. Recall that in the RP, two types of CB responses are generated: the transient CB response after a sustained change in BCL (CB-D) and the transient CB response to a perturbation in BCL (CB-S). Experimentally, and in the RP of Fig. 1, neither of these types of CB responses form a single curve; they both initially oscillate before slowly reaching steady state. The eigenvalue

analysis of this specific mapping, as well as a graphical visualization, are presented here to illustrate how these CB transients are generated.

For a mapping model with only two D variables, Eq. (21) is rewritten as

$$A_{n+1} = \Phi(D_n, D_{n-1}). \tag{32}$$

This mapping describes any responses to pacing at B , the same BCL used to determine the fixed point indicated by the star in Fig. 5, and used to generate the S1-S2 RC in Fig. 6. Similar to the mappings Ψ and Ω , Φ can also be plotted as a two-dimensional surface as in Fig. 7. During constant pacing, all responses must fall on this surface, and a different surface exists for each BCL.

For this specific mapping, the linearized equation (23) can be rewritten as

$$\begin{pmatrix} \delta_{n+1} \\ \delta_n \end{pmatrix} = \begin{pmatrix} -\eta & -\rho \\ 1 & 0 \end{pmatrix} \begin{pmatrix} \delta_n \\ \delta_{n-1} \end{pmatrix}, \tag{33}$$

where $\eta = \partial\Phi/\partial D_n|_{fp}$ and $\rho = \partial\Phi/\partial D_{n-1}|_{fp}$. The eigenvalues of the 2×2 matrix given in Eq. (33) are

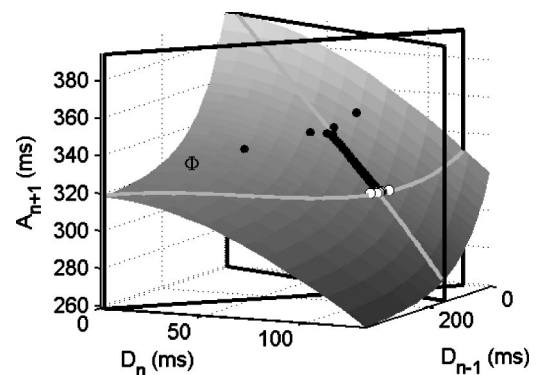


FIG. 7. Visualization of the CB responses. The shaded surface is the surface Φ . The two planes outlined in black correspond to the two eigendirections of the 2×2 matrix given in (33). The intersection of each of these planes with the surface Φ (gray curves) governs the behavior of the transient CB responses. The filled black circles show the CB-D responses that occur when the BCL is changed from 500 to 400 ms. The filled white circles show CB-S responses that occur after perturbations are applied at BCL ± 10 ms. The intersection of the two gray curves occurs at the steady-state value $A_*^B = \Phi(D_*^B, D_*^B)$ for the BCL $B=400$ ms. The specific form of Φ is given as (A8) in the Appendix.

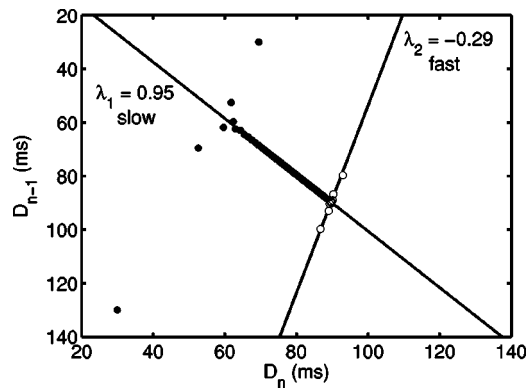


FIG. 8. Eigendirections and associated eigenvalues shown in the $(D_n - D_{n-1})$ plane. The CB-D responses (filled circles) and CB-S responses (open circles) are also shown in this plot, illustrating how the directions of the two eigenvectors determine the CB responses.

$$\lambda_{1,2} = \frac{1}{2}(-\eta \pm \sqrt{\eta^2 - 4\rho}). \quad (34)$$

For a given eigenvalue λ_n eigenvector $V_n = (v_1, v_2)$ satisfies

$$\begin{pmatrix} -\eta - \lambda_n & -\rho \\ 1 & -\lambda_n \end{pmatrix} \begin{pmatrix} v_1 \\ v_2 \end{pmatrix} = \begin{pmatrix} 0 \\ 0 \end{pmatrix}. \quad (35)$$

The eigendirections spanning these eigenvectors are shown in the $(D_n - D_{n-1})$ plane along with their associated eigenvalues in Fig. 8 for the particular mapping used to generate the surface Φ in Fig. 7. Note that Fig. 8 shows a bird's eye view of the $(D_n - D_{n-1})$ plane and therefore, D_{n-1} increases in a downward direction.

An eigenvalue λ describes the decay of a perturbation δ as $\delta_n = \lambda^n \delta_0$. Therefore, eigenvalues close to 1 describe very slow decay and eigenvalues close to zero describe fast decay. For the particular mapping shown here, there is a slow eigenvalue/vector ($\lambda_1 = 0.95$) and a fast eigenvalue/vector ($\lambda_2 = -0.29$). The Appendix includes an explanation of the origins of these eigenvalues for this particular mapping. The (D_n, D_{n-1}) values for CB-D and CB-S responses are also shown in Fig. 8. The CB-D responses show this initial fast response followed by a slow response along the direction of the slow eigenvector. The CB-S response is dominated by the fast eigenvector. The response governed by the slow eigenvector gives rise to the observation of accommodation, the slow change in APD that accompanies a change in BCL. Accommodation has been observed in superfused^{9,23,24} and perfused²⁵ experimental tissue preparations, in single-cell experimental preparations,²⁶ in clinical in-vivo human ventricular recordings,²⁷ and in ionic models of cardiac membrane.²⁸⁻³⁰ Mapping models that reproduce accommodation will have both fast and slow eigenvalues, while those models that do not reproduce accommodation will have eigenvalues that are more similar in magnitude.

In Fig. 7, vertical planes associated with these two eigendirections are shown as they intersect the surface Φ . The (D_n, D_{n-1}) values shown in Fig. 8 are also mapped to the surface Φ , demonstrating how these eigendirections govern the behavior of the CB responses. The specific example presented in Fig. 7 is for a three-variable model [$m=2$ for the matrix in Eq. (23)], where the CB surface Φ can be graphi-

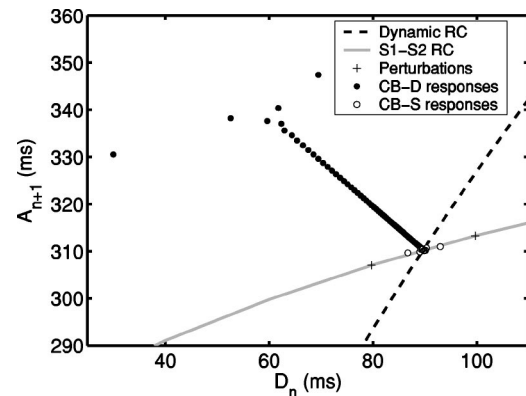


FIG. 9. Superposition of projections of different RCs onto the $(A_{n+1} - D_n)$ plane. Responses to perturbations of BCL ± 10 ms are shown on the S1-S2 RC. The CB-D responses show the transient that occurs in decreasing the BCL from 500 to 400 ms. The CB-S responses show the recovery from the perturbations.

cally represented. For a model with only one D variable ($m=1$), the expression given in (21) can also be represented graphically; however, it describes a curve, rather than a surface. For models with $m > 2$ D variables, the expression in (21) forms an m -dimensional hypersurface and all CB responses must fall on that hypersurface. Note that, for any number of D variables, the CB responses in the RP are the projection of the responses onto the $(A_{n+1} - D_n)$ plane.

D. Simultaneous projection onto $(A_{n+1} - D_n)$ plane

All of the surfaces Ψ , Ω , and Φ have the axes D_n and A_{n+1} in common. (For the surfaces Ψ and Ω , D_* and D_{S2} represent D_n , respectively.) Therefore, the 3D-DRC, 3D-SRC, and transient CB responses described above can be projected simultaneously onto the $(A_{n+1} - D_n)$ plane to show the parts of the RP for a given BCL (Fig. 9). The stars in Figs. 5 and 6 show the point where the RCs intersect in this projection. This superposition of projections differs from an RP obtained using the perturbed downswEEP protocol experimentally or in iterating a model (Fig. 2). This is because only segments of these RCs around the fixed points are obtained in applying the perturbed downswEEP protocol. It is only these segments around the fixed point that are necessary to evaluate the stability of the response.

This graphical visualization demonstrates how each component of the RP represents a different section of the space of variables of the mapping model (4). Each subspace of variables is projected onto the $(A_{n+1} - D_n)$ plane to form the RP as shown in Fig. 9. The dynamic and S1-S2 RCs reside on two-dimensional subspaces, regardless of the degree of memory in the mapping model (4). However, the CB transient responses reside on an m -dimensional subspace. From the determination of the different subspaces presented in Secs. IV A-IV C, we see why there will be one dynamic RC over all BCLs, one S1-S2 RC for each fixed point, and CB responses that will not necessarily be represented by a single curve for higher-dimensional mappings.

V. DISCUSSION

In this paper, we have interpreted experimentally measured RCs in the framework of mapping models with arbitrary degrees of memory. Although we have presented this interpretation in the context of the RP, this analysis also applies for typical dynamic and S1–S2 pacing protocols when slopes are measured around the fixed point. We used analytical and graphical techniques to collapse higher-dimensional mapping models to the number of variables necessary to determine the dynamic and S1–S2 RCs and the CB transient responses. We have found that the slope of the dynamic RC depends on the amount of memory in the model, while the slope of the S1–S2 RC does not. We also found that CB responses belong to an m dimensional space, where m is the number of D variables in the model. While this work has focused on the 1:1 regime of possible responses, it may be possible to extend the graphical techniques developed here to better understand other behaviors, such as the 2:2 response.

It is important to note that in this study we assume that cardiac dynamics are described by a model of the form (4). Previously, models of this form were derived empirically from experimental data.^{10,11,20} More recently, it has been shown that some ionic models consisting of ODEs (representing transmembrane voltage and channel gating variables) can be approximated as mapping models of the form (4). For example, it was shown that the Fenton–Karma simplified ionic model can be approximated as a two-variable mapping.¹⁹ Similarly, it was shown that a new two-current simplified ionic model that includes a concentration variable can be represented as a three-variable mapping.¹² Therefore, it is possible that mapping models of the form (4) with more memory variables may approximate more detailed models of cardiac membrane, and thus reproduce experimental results more completely. Indeed, we have found that increasing the amount of memory in the mapping model from two to three variables has led to closer agreement with experimental results.⁹ Models that include even more memory may provide even better agreement with experiments, especially in prediction of alternans.

We recognize that it is also quite possible that development of a new type of mapping model of a different form may accomplish this task. For example, recent studies have suggested that the appearance of alternans is related to intracellular calcium cycling, rather than APD restitution.^{31,32} While it is possible that a mapping model of the form (4) with enough variables can include effects of intracellular calcium cycling, it also may be necessary or expedient to include variables other than APDs and DIs in a mapping model. For example, such variables may include uptake and release of calcium from the sarcoplasmic reticulum as recently proposed by Shiferaw *et al.*³³ For any new model, it will be necessary to interpret the experimentally measured restitution curves as we have done here in order to understand the physical significance of each of the protocols used in practice. However, to date, no other such models have been completely developed, and therefore it is important to understand the RCs for the most common types of mapping models.

The results of this study may have important implications for measuring restitution in practice. Modeling and experimental studies typically use S1–S2 and dynamic protocols. Our analysis shows that these two RCs reside on two-dimensional surfaces, regardless of the dimension of the mapping model. Therefore, these two common protocols cannot be used to assess whether cardiac dynamics are described by models with more than two variables. Moreover, criteria for the onset of alternans based only on S_{12} or S_{dyn} have had only mixed success when applied to experimental data.^{20,34,35}

In this regard, the CB transients, which are usually disregarded during dynamic and S1–S2 protocols, may prove to be of practical use. First, they may lead to a more reliable criterion for alternans. The first step in this direction is the study by Tolkacheva *et al.*, who demonstrated the importance of CB responses for prediction of alternans in a three-variable model.¹⁴ Specifically, this study showed that the criterion for alternans for a three-variable model cannot be expressed in terms of only S_{12} and S_{dyn} , while it can for the one- and two-variable models.^{5,8}

Second, the CB responses are the only component of the RP that depends on higher-dimensional memory. Thus, they may lead to a practical method of determining the dimensionality of cardiac dynamics. For example, the sequential APD and DI data can be embedded into increasingly higher dimensions to determine if the CB responses fall on an m -dimensional surface. We conjecture that such analysis would provide a means of estimating a lower bound on the dimension of cardiac dynamics.

The importance of the CB responses was also seen in our previous study, in which CB responses revealed that a two-variable model does not describe experimental observations adequately. Specifically, a two-variable model predicts that there is a unique CB RC for each BCL and therefore, transient responses will fall on this curve. However, CB responses did not fall on one curve experimentally, and our analysis demonstrates the reason for it. In the model (2), the possible CB responses are described by a surface in D_n and D_{n-1} . With the dependence on D_{n-1} , the projection of the CB surface onto the $(A_{n+1}-D_n)$ plane will have some extent in A_{n+1} for a given D_n , and CB responses will fall within this extent in a manner that depends on the protocol. If there were no dependence on D_{n-1} , as is the case for the two-variable model, all CB responses would fall on a single curve when projected in the $(A_{n+1}-D_n)$ plane. However, with the dependence on D_{n-1} , the CB responses are governed by the eigenvalues and eigenvectors of the mapping for a particular BCL, and do not fall on a single curve.

As we begin to find that cardiac dynamics cannot be represented by simple unidimensional mappings, we are faced with increasingly complex models. Experimentally measured RCs only show such dynamics through one section of the space represented by a mapping model, i.e., the $(A_{n+1}-D_n)$ plane. Therefore, intuitive understanding of the RCs and expected dynamical behavior becomes difficult. In this regard, this analysis of models with an arbitrary degree of memory may give rise to better experimental pacing protocols. These protocols will rely less on the dynamic and

S1–S2 RCs that yield limited information about cardiac dynamics. Instead, they will be designed to utilize the CB transient responses that hold valuable information regarding the degree of memory present in the system.

ACKNOWLEDGMENTS

The authors gratefully acknowledge the financial support of the National Institutes of Health under Grant No. 1R01-HL-72831 and the National Science Foundation under Grant No. PHY-0243584.

APPENDIX: MODEL EQUATIONS

While the results presented in this paper apply to general models of the form (4), a specific model was used to generate the graphics used for illustration. The model used was developed by Gulrajani,¹¹ and specifically formulated by Chialvo *et al.*¹⁰ and Fox *et al.*,²²

$$A_{n+1} = (1 - \alpha M_{n+1})G(D_n), \quad (\text{A1})$$

$$M_{n+1} = [1 - (1 - M_n)e^{-A_n/\tau_2}]e^{-D_n/\tau_2}, \quad (\text{A2})$$

where we use the form of $G(D_n)$ presented by Chialvo *et al.*,

$$G(D_n) = a_1 - a_2 e^{-D_n/\tau_1}. \quad (\text{A3})$$

Tolkacheva *et al.*¹⁴ showed that the model given by (A1)–(A3), can be expressed as a three-variable mapping. Based on the derivation presented therein, this three-variable mapping can be written as

$$F(D_n, A_n, D_{n-1}) = \left[1 - \alpha e^{-D_n/\tau_2} + \left(\alpha - 1 + \frac{A_n}{G(D_{n-1})} \right) \times e^{-(A_n + D_n)/\tau_2} \right] G(D_n). \quad (\text{A4})$$

For the simulations, we used parameters previously given in Ref. 9 that reproduce the qualitative features of the experimental bullfrog heart RP, $a_1 = 1500$ ms, $a_2 = 300$ ms, $\tau_1 = 100$ ms, $\alpha = 1$, and $\tau_2 = 30\,000$ ms. For determination of the S1–S2 RC and transient CB responses, a BCL of 400 ms is used in the following equations where the term B appears.

Dynamic RC

The specific expression used for the surface Ψ is given by

$$\Psi(A_*, D_*) = (1 - \alpha M_*)G(D_*), \quad (\text{A5})$$

where

$$M_* = \frac{e^{-D_*/\tau_2}(1 - e^{-A_*/\tau_2})}{1 - e^{-(A_* + D_*)/\tau_2}}. \quad (\text{A6})$$

S1–S2 RC

The expression used for the surface Ω is given by

$$\Omega(D_{S2}, D_*) = \left[1 - \alpha e^{-D_{S2}/\tau_2} + \left(\alpha - 1 + \frac{B - D_*}{G(D_*)} \right) \times e^{-(B - D_*) + D_{S2}/\tau_2} \right] G(D_{S2}). \quad (\text{A7})$$

Transient CB responses

The expression used for the surface $\Phi(D_n, D_{n-1})$ is given by

$$\Phi(D_n, D_{n-1}) = \left[1 - \alpha e^{-D_n/\tau_2} + \left(\alpha - 1 + \frac{B - D_n}{G(D_{n-1})} \right) e^{-B/\tau_2} \right] G(D_n). \quad (\text{A8})$$

The following are the expressions for the partial derivatives of Φ with respect to D_n and D_{n-1} , respectively,

$$\eta = \left. \frac{\partial G}{\partial D_n} \right|_{\text{fp}} (1 - \alpha M_*) + G(D_*^B) \left(\frac{\alpha}{\tau_2} e^{-D_*^B/\tau_2} - \frac{e^{-B/\tau_2}}{G(D_*^B)} \right), \quad (\text{A9})$$

$$\rho = - \left. \frac{\partial G}{\partial D_n} \right|_{\text{fp}} (1 - \alpha M_*) e^{-B/\tau_2}, \quad (\text{A10})$$

where M_* is defined in (A6).

Eigenvalues for the three-variable mapping

The eigenvalues of a mapping model will depend on mapping model parameters. If parameters are chosen to reproduce accommodation, there will be at least two different time scales, one fast and one slow. For the particular model studied here (A1)–(A3), the memory variable M is responsible for accommodation with a time constant on the order of τ_2 . For this model, the assumption of long τ_2 allows some analysis regarding the origins of the two different time scales.

Assumption of long τ_2 (\gg BCL) allows the map equations (A1)–(A3) to be written as

$$A_{n+1} = (1 - \alpha M_{n+1})G(D_n), \quad (\text{A11})$$

$$M_{n+1} = M_n \left(1 - \frac{B}{\tau_2} \right) + \frac{A_n}{\tau_2}, \quad (\text{A12})$$

where $B = A_n + D_n$. The Jacobian of this mapping can be written in the form $J = J_0 + \varepsilon J_1$ as

$$J = \begin{pmatrix} -(1 - \alpha M_*)G'(D_*) & -\alpha G(D_*) \\ 0 & 1 \end{pmatrix} + \frac{1}{\tau_2} \begin{pmatrix} 0 & 0 \\ 1 & -B \end{pmatrix}, \quad (\text{A13})$$

where ε is $1/\tau_2$, and J_0 and J_1 are the two 2×2 matrices. Therefore, if τ_2 is large (as it must be to produce accommodation), the eigenvalues of J are equal to the eigenvalues of J_0 plus some small correction: $-(1 - \alpha M_*)G'(D_*) + \varepsilon_1$ (fast eigenvalue) and $1 + \varepsilon_2$ (slow eigenvalue), where ε_1 and ε_2 are small and can be determined by perturbation theory. Therefore, the slow eigenvalue is close to 1, independent of pa-

rameters α , a_1 , a_2 , and τ_1 ; while the fast eigenvalue depends on all parameters. Incidentally, it can also be shown that $S_{12} \approx (1 - \alpha M^*)G'(D^*)$, and therefore, the fast eigenvalue will also be approximated by S_{12} for this particular model under the long τ_2 assumption.

- ¹M. Courtemanche, R. J. Ramirez, and S. Nattel, "Ionic mechanisms underlying human atrial action potential properties: insights from a mathematical model," *Am. J. Physiol.* **275**, H301–H321 (1998).
- ²C.-H. Luo, and Y. Rudy, "A dynamic model of the cardiac ventricular action potential. i. simulations of ionic currents and concentration changes," *Circ. Res.* **74**, 1071–1096 (1994).
- ³A. Nygren, C. Fiset, L. Firek, J. W. Clark, D. S. Lindblad, R. B. Clark, and W. R. Giles, "Mathematical model of an adult human atrial cell," *Circ. Res.* **82**, 63–81 (1998).
- ⁴J. W. Nolasco, and R. W. Dahlen, "A graphic method for the study of alternation in cardiac action potentials," *J. Appl. Physiol.* **25**, 191–196 (1968).
- ⁵M. R. Guevara, G. Ward, and L. Glass, "Electrical alternans and period-doubling bifurcations," in *Proceedings of Computers in Cardiology*, edited by K. Ripley (IEEE Computer Society Press, Washington, DC, 1984), pp. 167–170.
- ⁶V. Elharrar, and B. Surawicz, "Cycle length effect on restitution of action potential duration in dog cardiac fibers," *Am. J. Physiol.* **244**, H782–H792 (1983).
- ⁷M. L. Koller, M. L. Riccio, and R. F. Gilmour, Jr., "Dynamic restitution of action potential duration during electrical alternans and ventricular fibrillation," *Am. J. Physiol.* **44**, H1635–H1642 (1998).
- ⁸E. G. Tolkacheva, D. G. Schaeffer, D. J. Gauthier, and W. Krassowska, "Condition for alternans and stability of the 1:1 response pattern in a 'memory' model of paced cardiac dynamics," *Phys. Rev. E* **67**, 031904 (2003).
- ⁹S. S. Kalb, H. Dobrovolny, E. G. Tolkacheva, S. F. Idriss, W. Krassowska, and D. J. Gauthier, "The restitution portrait: A new method for investigating rate-dependent restitution," *J. Cardiovasc. Electrophysiol.* **15**, 698–709 (2004).
- ¹⁰D. R. Chialvo, D. C. Michaels, and J. Jalife, "Supernormal excitability as a mechanism of chaotic dynamics of activation in cardiac purkinje fibers," *Circ. Res.* **66**, 525–545 (1990).
- ¹¹R. M. Gulrajani, "Computer simulation of action potential changes in cardiac tissue," in *Proceedings of Computers in Cardiology*, edited by K. Ripley (IEEE Computer Society Press, Washington, DC, 1987), pp. 629–632.
- ¹²D. G. Schaeffer, J. W. Cain, D. J. Gauthier, S. S. Kalb, W. Krassowska, R. A. Oliver, and E. G. Tolkacheva, "An ionically based mapping model with memory for cardiac restitution," arXiv: q-bio.QM/0407016, 2004.
- ¹³Previously, Tolkacheva *et al.* (Ref. 14) referred to the slope of the CB RC (S_{bc}) for the three-variable model of the form (2) as the slope formed by the CB–S responses. However, for the model (2), the CB–S responses do not fall on a single curve. Therefore, we clarify here that the slope (S_{bc}) in Ref. 14 refers to the slope formed by those CB–S responses immediately following each of the perturbations.
- ¹⁴E. G. Tolkacheva, M. M. Romeo, M. Guerraty, and D. J. Gauthier, "Condition for alternans and its control in a two-dimensional mapping model of paced cardiac dynamics," *Phys. Rev. E* **69**, 031904 (2004).
- ¹⁵M. Courtemanche, L. Glass, and J. P. Keener, "Instabilities of a propagating pulse in a ring of excitable media," *Phys. Rev. Lett.* **70**, 2182–2185 (1993).
- ¹⁶A. Vinet and F. A. Roberge, "Excitability and repolarization in an ionic model of the cardiac cell membrane," *J. Theor. Biol.* **170**, 183–199 (1994).
- ¹⁷A. Vinet, and F. A. Roberge, "Analysis of an interactive difference equation model of the cardiac cell membrane," *J. Theor. Biol.* **170**, 210–214 (1994).
- ¹⁸Z. Qu, A. Garfinkel, P.-S. Chen, and J. N. Weiss, "Mechanisms of discordant alternans and induction of reentry in simulated cardiac tissue," *Circulation* **102**, 1664–1671 (2000).
- ¹⁹E. G. Tolkacheva, D. G. Schaeffer, D. J. Gauthier, and C. C. Mitchell, "Analysis of the Fenton–Karma model through an approximation by a one-dimensional map," *Chaos* **12**, 1034–1042 (2002).
- ²⁰R. F. Gilmour, Jr., N. F. Otani, and M. A. Watanabe, "Memory and complex dynamics in cardiac Purkinje fibers," *Am. J. Physiol.* **272**, H1826–H1832 (1997).
- ²¹N. F. Otani, and R. F. Gilmour, Jr., "Memory models for the electrical properties of local cardiac systems," *J. Theor. Biol.* **187**, 409–436 (1997).
- ²²J. J. Fox, E. Bodenschatz, and R. F. Gilmour, Jr., "Period-doubling instability and memory in cardiac tissue," *Phys. Rev. Lett.* **89**, 138101 (2002).
- ²³M. A. Watanabe, and M. L. Koller, "Mathematical analysis of dynamics of cardiac memory and accommodation," *Am. J. Physiol.* **282**, H1534–H1547 (2002).
- ²⁴M. R. Boyett and B. R. Jewell, "Analysis of the effects of changes in rate and rhythm upon electrical activity in the heart," *Prog. Biophys. Mol. Biol.* **36**, 1–52 (1980).
- ²⁵S. F. Idriss and A. M. Pitruzzello (perfused rabbit ventricular myocardium) (private communication).
- ²⁶E. G. Tolkacheva (unpublished).
- ²⁷M. R. Franz, C. D. Swerdlow, L. L. Bing, and J. Schaefer, "Cycle length dependence of human action potential duration in vivo," *J. Clin. Invest.* **82**, 972–979 (1988).
- ²⁸S. S. Kalb, J. J. Fox, E. G. Tolkacheva, D. J. Gauthier, and W. Krassowska, "Parameter estimation in mapping models with memory (unpublished).
- ²⁹R. A. Oliver, A. W. Wood, S. S. Kalb, and W. Krassowska, "Restitution portrait in Luo–Rudy-dynamic cardiac membrane model," *Proceedings of the 2004 BMES Annual Fall Meeting* (Biomedical Engineering Society, Philadelphia, PA, 2004).
- ³⁰T. J. Hund, J. P. Kucera, N. F. Otani, and Y. Rudy, "Ionic charge conservation and long-term steady-state in the Luo–Rudy dynamic cell model," *Biophys. J.* **81**, 3324–3331 (2001).
- ³¹M. E. Díaz, S. C. O'Neill, and D. A. Eisner, "Sarcoplasmic reticulum calcium content fluctuation is the key to cardiac alternans," *Circ. Res.* **94**, 650–656 (2004).
- ³²E. J. Pruvot, R. P. Katta, D. S. Rosenbaum, and K. R. Laurita, "Role of calcium cycling versus restitution in the mechanism of repolarization alternans," *Circ. Res.* **94**, 1083–1090 (2004).
- ³³Y. Shiferaw, D. Sato, and A. Karma, "Coupled dynamics of voltage and calcium in paced cardiac cells," arXiv: physics/0405048, 2004.
- ³⁴G. M. Hall, S. Bahar, and D. J. Gauthier, "Prevalence of rate-dependent behaviors in cardiac muscle," *Phys. Rev. Lett.* **82**, 2995–2998 (1999).
- ³⁵I. Banville, and R. A. Gray, "Effect of action potential duration and conduction velocity restitution and their spatial dispersion on alternans and the stability of arrhythmias," *J. Cardiovasc. Electrophysiol.* **13**, 1141–1149 (2002).